WILEY | Hindawi

Research Article

Characterization of Refractory Alloys Produced by Laser Additive Manufacturing

Andrew B. Kustas ,[1] Jonathan Pegues ,[1] Michael A. Melia ,[1] Shaun R. Whetten,[1] Morgan Jones ,[1,2] and Nicolas Argibay [3]

[1]*Material, Physical, and Chemical Sciences Center, Sandia National Laboratories, Albuquerque, NM, USA*
[2]*Materials Department, University of California, Santa Barbara, CA, USA*
[3]*Ames National Laboratory, Iowa State University, Ames, IA, USA*

Correspondence should be addressed to Andrew B. Kustas; akustas@sandia.gov

Refractory alloys often possess superior thermomechanical properties compared to conventional materials, such as steels, Ni-based superalloys, and Ti alloys, especially in high-temperature environments. While these materials promise to revolutionize numerous industries, significant hurdles remain for insertion into applications due to an incomplete understanding of structure-property relationships and conventional processing challenges. We explore laser-based additive manufacturing (AM) to construct refractory alloys consisting of combinations of Mo, Nb, Ta, and Ti with systematically increasing compositional complexity. Microstructure, composition, and hardness of the AM-processed alloys were characterized. Results are discussed in the context of pairing additive manufacturing with refractory metals to enable next-generation alloys.

1. Introduction

Refractory alloys (RAs) possess extraordinary properties relative to conventional materials, such as steels, Ni-based superalloys, and Ti alloys, making them compelling candidates for use in elevated temperature structural applications. This is especially true for refractory complex-concentrated alloys (RCCAs), which are a subset of RAs that consist of four or more elements (e.g., Mo, Nb, Ta, Ti, and W) each with a significant atomic fraction of nominally 5 to 35 at.%. RAs/RCCAs have shown promise as next-generation materials for use in harsh operating conditions, such as at high temperatures, in corrosive and oxidizing atmospheres, and in radiation environments. Examples include aerospace propulsion systems, gas turbines, nuclear reactors, heat exchangers, and rocket engine nozzles [1].

Despite their potential to revolutionize numerous industries, successful widespread adoption of RAs and RCCAs in commercial applications remains limited. This is largely due to an incomplete understanding of structure-property relationships and conventional processing challenges when manufacturing these alloys [2]. Most studies have evaluated structure-mechanical property relationships of RAs/RCCAs produced via conventional techniques, such as induction melting, powder metallurgy techniques, or thin coatings [1]. By comparison, far fewer studies have evaluated the properties of these materials produced via alternative, advanced manufacturing methods. Additive manufacturing (AM) in particular provides unique opportunities for constructing near-net-shape bulk geometries from complex refractory alloys, which can be impractical to conventionally manufacture due to poor material workability and high melting temperatures. Few reports have examined additive manufacturing of RAs/RCCAs [3–10].

In this study, we utilized the Laser Beam Directed Energy Deposition (LB-DED) AM process to produce bulk RA/RCCA specimens with varying compositions produced from elemental Mo, Nb, Ta, and Ti powders. The composition, microstructure, and hardness of the AM-processed alloys were evaluated and are discussed in the context of

accelerating the development and application insertion opportunities of RAs/RCCAs via advanced manufacturing.

2. Materials and Methods

A range of alloys were constructed using elemental powder feedstock of Mo, Nb, Ta, and Ti. Additional details on the powder feedstock are available in the supplemental. Specimens were constructed from premixed elemental powders within a single powder reservoir, targeting an initially equiatomic composition from NbTa, NbTaTi, MoNbTa, and MoNbTaTi alloys, the latter of which fits the traditional RCCA definition. An open-architecture DED AM system was used to consolidate the powders, which is described in detail in ref. [11]. A series of vertical square rod specimens were produced using LB-DED that were 5 mm^2 in cross-section and 52 mm in length (parallel to the build direction) with a range of processing conditions depending on alloy composition (see Table S1 in the supplemental for details). Specimens were constructed on a Ti build substrate plate that was actively heated to ~200°C to limit cracking. A constant layer thickness of 250 μm was used with an approximate beam diameter of 1 mm.

Specimens for microstructural characterization were mounted in cold set epoxy and cross-sectioned, parallel to the build direction. Grain structure was characterized using electron backscatter diffraction (EBSD), while hardness was determined via Vickers microindentation and microscratch testing. Full details on the metallographic preparation steps and methods for microstructure/properties characterization are available in the supplemental.

3. Results and Discussion

Large-area EBSD maps for the four alloys are shown in Figure 1. Defect density, specifically areal fraction of porosity and unmelted powder, was generally higher for specimens with an increased compositional complexity. The four-constituent MoNbTaTi RCCA, in particular, showed notable mm-sized macroscopic porosity at the center of the part, while the three- and two-component RAs—NbTaTi, MoNbTa, and NbTa—exhibited comparably finer porosity in the ~100 μm (or smaller) size range. Despite the porosity, no significant macroscopic cracking from low alloy workability was observed in any specimen, which is a distinct improvement in manufacturing quality when compared to recent studies by the current authors on AM-processed RCCAs [12, 13]. Absence of macroscopic cracking was likely due to a combination of processing and alloying factors. For processing, the use of a Ti build plate and an elevated substrate temperature during synthesis likely improved thermal stress management. In terms of alloy selection, compositions with varying average valence electron concentration (VEC) of 4.58, 5.33, 5, and 4.83 were produced for the NbTa, MoNbTa, NbTaTi, and MoNbTaTi alloys, respectively. These values were calculated following a procedure outlined in ref. [12]. Recent studies have suggested that alloys with a lower VEC (<4.6) can promote *intrinsic ductility* for BCC-based RAs/RCCAs [14, 15].

Representative higher magnification EBSD color maps of the RA/RCCA specimens are shown in Figure 2. Alloys possessed a primarily equiaxed grain structure indexed by a single BCC lattice with limited evidence of epitaxial solidification. This is particularly pronounced for the Ti-containing specimens that possessed a greater extent of defects/porosity, which are known to interrupt epitaxial solidification often associated with layerwise AM processing [16]. The ternary alloys showed lack of fusion directly along melt pool boundaries where epitaxial solidification would be expected. Furthermore, notable differences in grain size were observed between alloys. The NbTa specimens possessed the largest grain size (d ~70 micron), while the MoNbTaTi specimen showed the finest structure (d ~35 micron). Reasons for the notable reduction in grain size with increased alloying content remain speculative, though it is evident that powder feedstock was less uniformly consolidated for the four-component alloy relative to the two- and three-component alloys. Grain size measurements generally support this hypothesis, which is shown in Figure S1 of the supplemental, and indicate a general decrease in average grain size with increased areal fraction of unmelted powder. Thus, a smaller grain size may have, in part, been inherited from the as-produced (unmelted) feedstock powder grain structure or via an enhanced number of nucleation sites from an increased volume fraction of unmelted powder [16]. The latter is more likely, since embedded powders in the specimens showed single grains in the maps of Figure 2. Interestingly, the extent of powder consolidation decreased in the NbTaTi and MoNbTaTi alloys, leaving behind a larger fraction of unmelted powder and an apparent bimodal distribution in grain size, one corresponding to the alloyed regions and the other reminiscent of the partially melted powder. This is likely the result of the selected processing conditions for the Ti-containing alloys, characterized by lower laser power to avoid excessive vaporization of Ti (Figure 2).

Alloyed regions of the specimens were reasonably close to the desired equiatomic composition, with the largest deviation observed for alloys that were processed with Ti (see Table S2 in the supplemental for average measured compositions). Specifically, the four-component alloy showed a Ti-content that was approximately 200% more abundant than the Mo refractory and nearly 150% more than the Nb and Ta elements. Similarly, the Ti-containing three-component alloy revealed a similar discrepancy with an approximate 150% increase in Ti-content relative to the Nb and Ta. The alloys without Ti were considerably closer to a true equiatomic composition. Nonetheless, all alloys represent unusually complex refractory compositions, fundamentally different to the conventional alloys utilized with AM. EBSD maps also revealed evidence of unmelted/partially melted powder particles embedded within the microstructures for all alloys, with the specific type of unmelted particle depending on the particular alloy composition and processing conditions utilized. In situ beamline experiments have recently shown the inherent difficulty in fully melting high-temperature refractory powder particles via laser-based additive processes and remain an ongoing challenge [17].
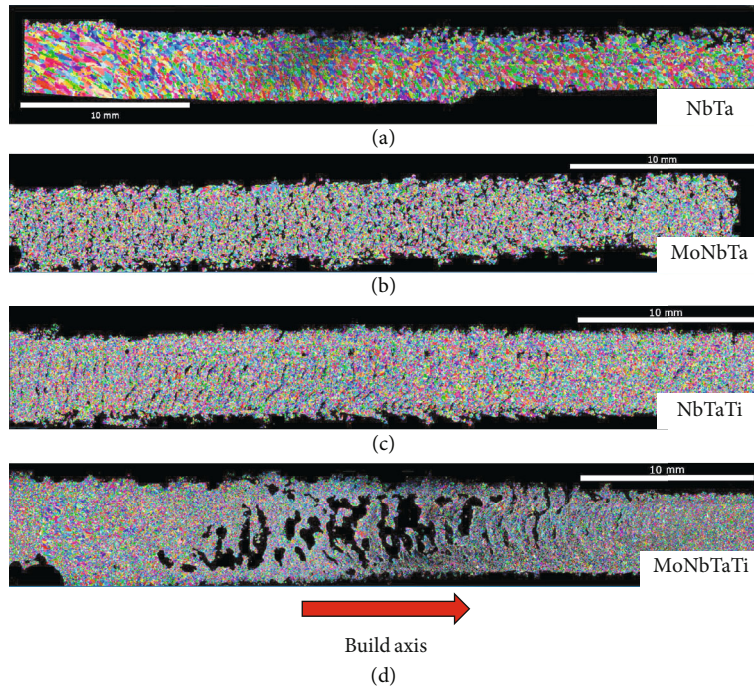
FIGURE 1: Representative large-area cross-sectional EBSD maps of the RA/RCCA rods.
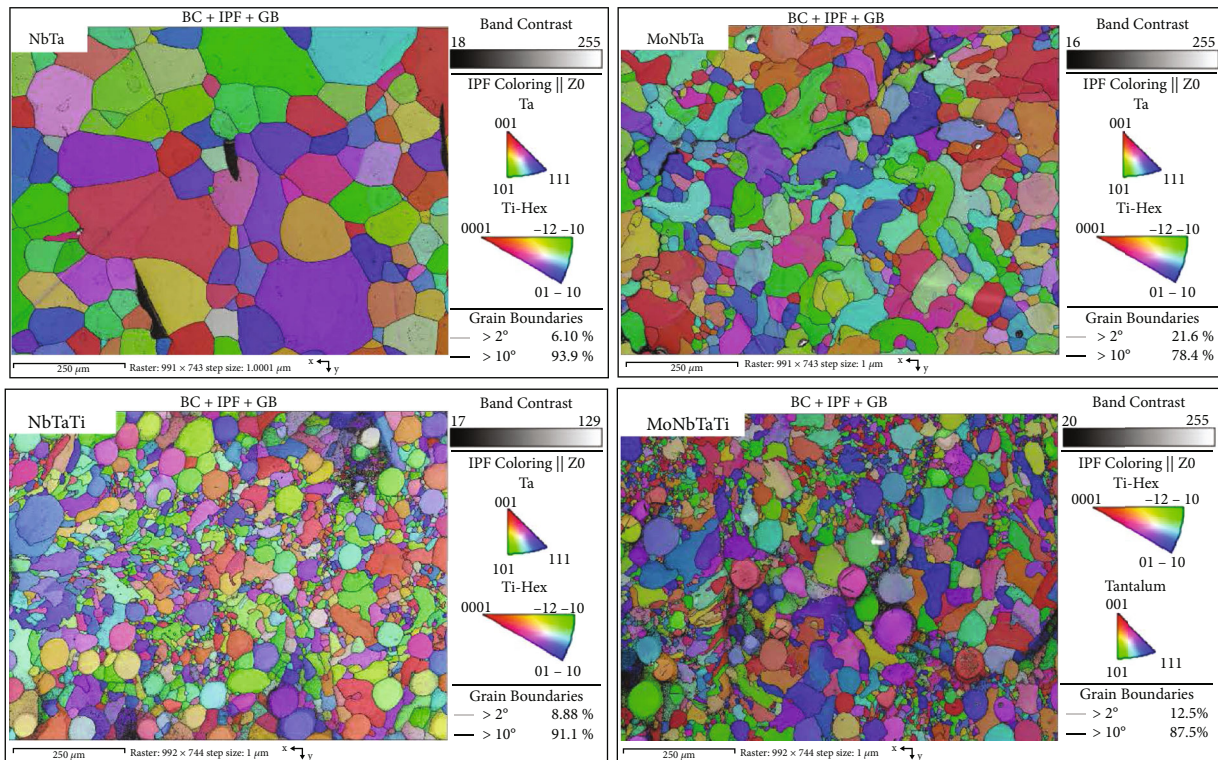

FIGURE 2: Representative grain structures of the RA/RCCA specimens.

Vickers microhardness results are shown in Figure 3 as spatial hardness maps for all four alloy compositions. In general, alloy hardness resided between ~200 and 500 HV. No particularly strong trend was observed between hardness and alloy composition, with the highest values observed for the ternary MoNbTa alloy, followed by MoNbTaTi, NbTa, and finally the NbTaTi. Additionally, specimens revealed mostly negligible gradients in hardness along specimen heights, indicating relatively homogeneous properties as a function of build location.
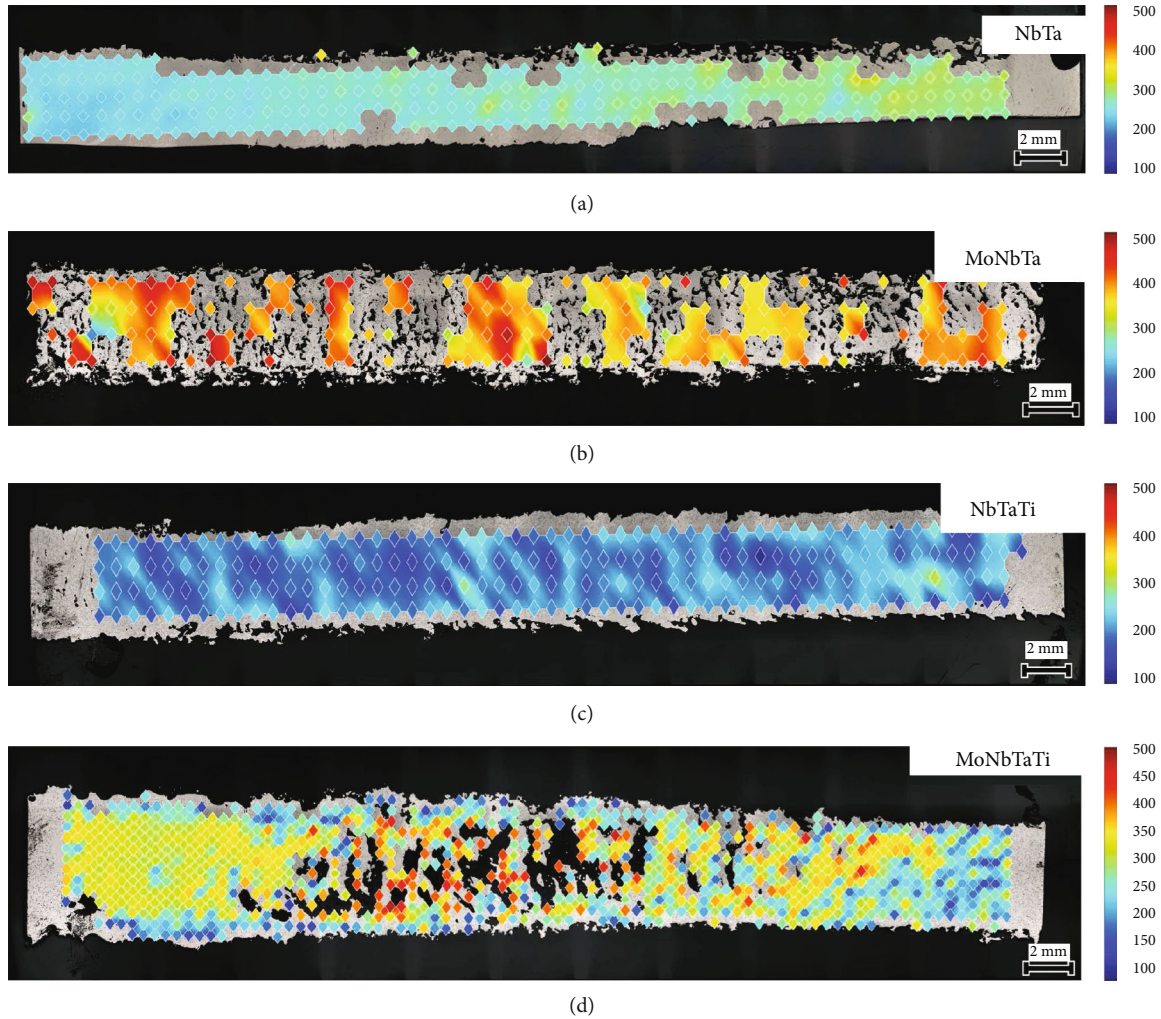
(a)

(b)

(c)

(d)

Figure 3: Spatial hardness maps for the RA/RCCA rods.

Hardness values were also determined via scratch testing over four orders of magnitude of strain rate and are plotted in a semilog form in Figure 4. The trends in hardness magnitude for each alloy composition generally agreed with the microhardness data. Over the strain rates evaluated, the alloys also exhibited similar linear strain rate-dependent hardness. The hardness vs. strain rate curves also revealed comparable strain rate sensitivities for the alloys, calculated as $m = \partial \ln(H)/\partial \ln(\dot{\varepsilon})$, with values of 0.078 +/-0.008, 0.097 +/-0.002, 0.110 +/-0.002, and 0.112 +/-0.006 for the MoNbTa, NbTa, MoNbTaTi, and NbTaTi alloys, respectively, suggesting typical dislocation-based deformation mechanisms. Notably, hardness values increased by more than 150% over the strain rates evaluated for all alloys and in some cases by nearly 250%. The similarity in strain rate-dependent hardness trends is not surprising given that the alloys were characterized by a single-phase BCC microstructure. BCC metals possess nonplanar dislocation cores, which are associated with rate-dependent Peierls-Nabarro stresses (lattice friction) during deformation, explaining the highly rate sensitive flow stress/hardness [18–20].

In acquiring hardness data, specimen defects were avoided as possible. This is evident for the Vickers results

in Figure 3, which show a lack of data near regions of excessive porosity. Similarly, wear track locations for the strain rate-dependent hardness scratch testing avoided defect-rich regions. However, both testing methods unavoidably evaluated regions of material that contained unmelted/partially melted powder, and thus, property data may have been influenced by the elemental feedstock. Despite these important nuances, hardness values presented in this study are in good agreement with recently published data for single-phase BCC AM-processed RCCAs [4, 12, 21].

Defect management and complete melting/incorporation of elemental powders are notable challenges in AM processing of refractory alloys, and future work in process optimization is needed to minimize these features. This is especially important when processing increasingly complex alloy compositions through the in situ AM alloying method employed in this study, where thermophysical properties of each powder feedstock need to be considered during selection of processing conditions. For instance, higher material quality was observed for the relatively simplistic binary alloy in this study, while the more complex four-component alloy showed the largest extent of process-induced defects likely due, in part, to the addition of Ti. Systematically evaluating
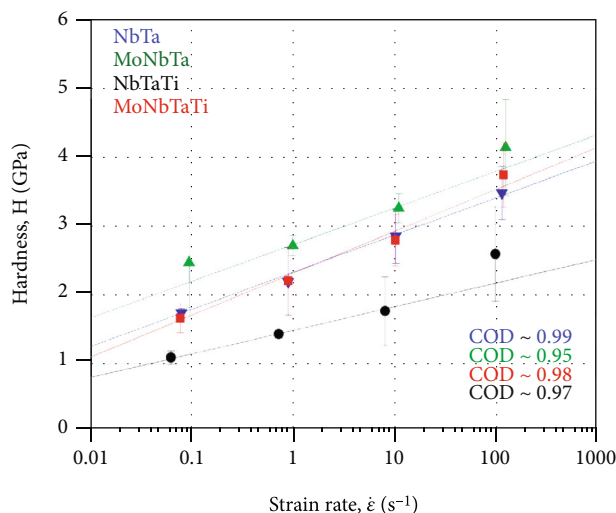
FIGURE 4: Hardness of each RA/RCCA plotted as a function of strain rate.

the role of processing parameters such as laser power, scan velocity, and hatch spacing across alloy compositions to minimize material heterogeneities is recommended and perhaps also including laser remelting steps similar to what is proposed in ref. [21]. Nonetheless, the methodology outlined in this study represents a potential and growing paradigm shift in the approach for next-generation alloy discovery. Among the principal advantages of this method is the opportunity to rapidly characterize performance of novel alloys using small material volumes. This combination of additive processing with local property measurements is advantageous to characterize the true structure-property relationships for novel refractory alloys by circumventing the effects of process-induced defects, as is demonstrated in the spatial hardness maps of this study wherein macroscopic porosity is avoided during the measurement. An accurate measure of the material properties is indeed crucial to informing alloy design and optimization models. Pairing advanced manufacturing methods with novel refractory alloys has the potential to enable opportunities for enhanced performance of numerous applications, including next-generation energy systems such as nuclear reactors and supercritical carbon dioxide Brayton cycles and transportation/aerospace systems (e.g., turbine engines) [22].

4. Conclusions

This study presented an approach to rapidly evaluate composition-dependent synthesis quality and mechanical properties by applying additive manufacturing and high-throughput mechanical testing methods to bulk refractory-based alloys consisting of varying Mo, Nb, Ta, and Ti compositions, including an alloy that satisfies the traditional RCCA definition. Specimens were characterized in terms of microstructure and mechanical (hardness) properties. Grain structure was primarily equiaxed for all alloys, with reduced size that was proportional to the areal fraction of unmelted

powder particles. SEM/EBSD images revealed an apparent bimodal grain size distribution for the Ti-containing alloys, suggested to be the result of having unique microstructures for both the alloy and partially melted powder feedstock. Hardness values of the AM-processed alloys ranged from approximately 200 to 500 HV and generally agreed with available peer-reviewed literature. Microscratch test results showed linear relationships between hardness and strain rate, varying from 1 to 4 GPa depending on the rate and alloy composition. Overall, defects inherited from processing are still a major issue impeding the commercialization opportunities of AM-processed refractory alloys, particularly for alloys composed of constituents with vastly different melting temperatures. Further work will be needed to reduce defects within AM-processed refractory alloys. Possible routes to do this include (1) altering the feedstock characteristics by pre-alloying the powder, improving flowability, and selecting elements with similar thermophysical properties and (2) optimizing machine process parameters to ensure full melting of powder feedstock.

Data Availability

Data is available on request.

Disclosure

Conflicts of Interest

The authors declare that they have no conflicts of interest.

Acknowledgments

Supplementary Materials

Table S1: RCCA processing conditions. Figure S1: measured grain size as a function of area fraction of unmelted powder for the 4 alloy compositions. Table S2: average RA/RCCA compositions (in at.%) [23]. (Supplementary Materials)

References

[1] O. N. Senkov, D. B. Miracle, K. J. Chaput, and J.-P. Couzinie, "Development and exploration of refractory high entropy alloys—a review," Journal of Materials Research, vol. 33, no. 19, pp. 3092–3128, 2018.

[2] Y. Zhang, J.-W. Yeh, J. F. Sun, J. P. Lin, and K.-F. Yao, "High-entropy alloys," vol. 2015, Article ID 10.1155/2015/781303, 1 pages, 2015.

[3] Q. Li, H. Zhang, D. Li et al., "WxNbMoTa refractory high-entropy alloys fabricated by laser cladding deposition," Materials, vol. 12, no. 3, pp. 1–14, 2019.

[4] H. Dobbelstein, M. Thiele, E. L. Gurevich, E. P. George, and A. Ostendorf, "Direct metal deposition of refractory high entropy alloy MoNbTaW," Physics Procedia, vol. 83, pp. 624–633, 2016.

[5] H. Dobbelstein, E. L. Gurevich, E. P. George, A. Ostendorf, and G. Laplanche, "Laser metal deposition of compositionally graded TiZrNbTa refractory high-entropy alloys using elemental powder blends," Additive Manufacturing, vol. 25, pp. 252–262, 2019.

[6] H. Dobbelstein, E. L. Gurevich, E. P. George, A. Ostendorf, and G. Laplanche, "Laser metal deposition of a refractory TiZrNbHfTa high-entropy alloy," Additive Manufacturing, vol. 24, pp. 386–390, 2018.

[7] M. Zhang, X. Zhou, X. Yu, and J. Li, "Synthesis and characterization of refractory TiZrNbWMo high-entropy alloy coating by laser cladding," Surface and Coatings Technology, vol. 311, pp. 321–329, 2017.

[8] I. Kunce, M. Polanski, and J. Bystrzycki, "Structure and hydrogen storage properties of a high entropy ZrTiVCrFeNi alloy synthesized using laser engineered net shaping (LENS)," International Journal of Hydrogen Energy, vol. 38, no. 27, pp. 12180–12189, 2013.

[9] I. Kunce, M. Polanski, and J. Bystrzycki, "Microstructure and hydrogen storage properties of a TiZrNbMoV high entropy alloy synthesized using laser engineered net shaping (LENS)," International Journal of Hydrogen Energy, vol. 39, no. 18, pp. 9904–9910, 2014.

[10] H. Zhang, Y. Zhao, S. Huang, S. Zhu, F. Wang, and D. Li, "Manufacturing and analysis of high-performance refractory high-entropy alloy via selective laser melting (SLM)," Materials, vol. 12, no. 5, 2019.

[11] A. B. Kustas, D. F. Susan, K. L. Johnson et al., "Characterization of the Fe-Co-1.5V soft ferromagnetic alloy processed by laser engineered net shaping (LENS)," Additive Manufacturing, vol. 21, pp. 41–52, 2018.

[12] M. A. Melia, S. R. Whetten, R. Puckett et al., "High-throughput additive manufacturing and characterization of refractory high entropy alloys," Applied Materials Today, vol. 19, article 100560, 2020.

[13] J. W. Pegues, M. A. Melia, R. Puckett, S. R. Whetten, N. Argibay, and A. B. Kustas, "Exploring additive manufacturing as a high-throughput screening tool for multiphase high entropy alloys," Additive Manufacturing, vol. 37, article 101598, 2021.

[14] S. Sheikh, S. Shafeie, Q. Hu et al., "Alloy design for intrinsically ductile refractory high-entropy alloys," Journal of Applied Physics, vol. 120, no. 16, article 164902, 2016.

[15] L. Qi and D. C. Chrzan, "Tuning ideal tensile strengths and intrinsic ductility of bcc refractory alloys," Physical Review Letters, vol. 112, no. 11, pp. 1–5, 2014.

[16] A. Basak and S. Das, "Epitaxy and microstructure evolution in metal additive manufacturing," Annual Review of Materials Research, vol. 46, no. 1, pp. 125–149, 2016.

[17] J. W. Pegues, M. A. Melia, M. A. Rodriguez et al., "In situ synchrotron X-ray imaging and mechanical properties characterization of additively manufactured high-entropy alloy composites," Journal of Alloys and Compounds, vol. 876, article 159505, 2021.

[18] Q. Wei, S. Cheng, K. T. Ramesh, and E. Ma, "Effect of nanocrystalline and ultrafine grain sizes on the strain rate sensitivity and activation volume: fcc versus bcc metals," Materials Science and Engineering A, vol. 381, no. 1-2, pp. 71–79, 2004.

[19] J. W. Edington, "The mechanical properties, dislocation substructure and density in niobium single crystals deformed at high strain rates," Philosophical Magazine, vol. 20, no. 165, pp. 531–538, 1969.

[20] R. W. K. Honeycombe, The Plastic Deformation of Metals, Edward Arnold, 1984.

[21] M. Moorehead, K. Bertsch, M. Niezgoda et al., "High-throughput synthesis of Mo-Nb-Ta-W high-entropy alloys via additive manufacturing," Materials and Design, vol. 187, article 108358, 2020.

[22] S. Rodriguez, A. Kustas, and G. Monroe, "Metal Alloy and RHEA Additive Manufacturing for Nuclear Energy and Aerospace Applications SAND 2020-7244," 2020, https://www.osti.gov/biblio/1644167%0Ahttps://www.osti.gov/servlets/purl/1644167.

[23] L. O. Nyakiti and A. F. Jankowski, "Characterization of strain-rate sensitivity and grain boundary structure in nanocrystalline gold-copper alloys," Metallurgical and Materials Transactions A, Physical Metallurgy and Materials Science, vol. 41, no. 4, pp. 838–847, 2010.